Unsteady Airloads Prediction for Oscillating Airfoils at Separated Flow Conditions

Coiro, D.P.
Università di Napoli "Federico II" - Italy

Pagano, A.
C.I.R.A. - Italy

20th ICAS Congress, 8-13 September 1996

Abstract

A viscous-inviscid interaction procedure for unsteady transonic flow using full potential and integral boundary layer equations is presented. Unsteady full potential equations have been used in both conservative and non conservative formulations. Unsteady compressible boundary layer equations are used both in direct and inverse forms and many different formulations of them are presented. Coupling between inviscid and viscous flow is performed using a semi-inverse approach. Steady coupling is performed using both conservative and non conservative full potential formulations. Unsteady coupling is performed using only non conservative full potential equations. The numerical results obtained for NLF and NACA0012 airfoils undergoing steady and unsteady motion are discussed and are compared with experiments.

Introduction

The prediction of aeroelastic behavior of modern aircraft cannot be performed without the capability of predicting unsteady transonic airloads on airfoils and wings.
The use of full Navier-Stokes equations to solve the unsteady problem is pratically forbidden due to the enourmous amount of computer time needed especially in a design phase when many load evaluations are necessary.
Assuming that the boundary layer equations adequately describe the viscous layer near the wall and that inviscid equations can be used to represent the external flow, these two regions may then be matched at a common boundary, usually the boundary layer edge. This type of approach is known as viscous/inviscid interaction and has been extensively used by one of the authors and in literature [1], [2], [3], [4],[5],[6], [7], [8] , [9], [10],[11].
This approach has been shown to be computationally inexpensive and accurate enough to also predict 2D flows when large areas of separation are present [12]. Thus coupling inviscid external flows to boundary layers appears attractive for the purposes just mentioned. In fact these relatively low-cost flow methods, provided that an accurate modelling of boundary layer is available, are able to predict viscous flows when strong interactions are present : separated flows, stall, strong shocks and subsequent shock-boundary layer interactions.
Transonic flow prediction is still an important task particularly for flutter speed prediction as in the transonic range a minimum of this speed occurs (the so called *transonic dip*). Furthermore for helicopter blade load prediction, due to the blade tip area being in transonic flow , the capability to predict aerodynamic characteristics in this Mach range is essential.
Most popular methods to compute inviscid unsteady transonic flows are based on Transonic Small Disturbance (TSD) equations which produce accurate solutions when moderate shocks are present and airfoils and wings are thin [13].
To overcome these limitations, unsteady full potential or Euler equations can be used. Unsteady Euler equations are still too demanding as far as computer time is concerned and full potential equations written in non conservative form (FPNC) along with those written in conservative form (FPC) have been used in this work.
One of the objectives of this paper is to compare and to analyse results obtained from both formulations. During the first stage of the work an inviscid FPNC code was coupled to an integral compressible boundary layer code using a semi-inverse algorithm and a quasi-steady coupling procedure. Due to the dissipative nature of inviscid non conservative formulation, when moderate or strong shock waves were present in the field, the coupling procedure led to erroneus results reducing the strength of shock waves too much and moving them unrealistically upstream.
The coupling was performed using for the inviscid flow the unsteady full potential equations written in conservative form and some of the previous mentioned problems were solved.
Furthermore unsteady integral boundary layer equations, written in direct and inverse form, have been solved and they will be discussed in a subsequent section; coupling of these equations to the inviscid ones

is necessary to obtain a true-unsteady interaction.

Inviscid Flow

For inviscid flow the unsteady full potential equation has been used both in conservative and non-conservative form. Both codes compute the development of two-dimensional unsteady subsonic or transonic flow about an airfoil in steady or unsteady motion.

Conservative formulation

The HELIFP-2D code, a two-dimensional version of the code HELIFP [14, 15] that predicts the aerodynamic flow around an isolated rotor blade, solves the unsteady full potential equation in conservative form:

$$\rho_t + (\rho u)_x + (\rho v)_y = 0 \tag{1}$$

The density ρ and the fluxes ρu and ρv are nonlinear functions of the velocity potential ϕ. The density is related to the potential by:

$$\rho = \left[1 - \frac{\gamma - 1}{2}\left(2\phi_t + u^2 + v^2\right)\right]^{\frac{1}{\gamma-1}}$$

The full potential equation may be written in curvilinear coordinates as:

$$\left(\frac{\rho}{J}\right)_\tau + \left(\frac{\rho}{J}U\right)_\xi + \left(\frac{\rho}{J}V\right)_\eta = 0 \ . \tag{2}$$

where J is the jacobian of the transformation and U and V are the contravariant velocity components.

In order to avoid non-physical solutions (expansion shocks) and stabilise the computation in supersonic flow regions, a streamwise density flux biasing is applied. In the full potential equation the density will be replaced by a biased density $\tilde{\rho}$ defined as

$$\tilde{\rho} = \rho - \frac{1}{qQ}\left[U\Delta\xi\frac{\partial}{\partial\xi} + V\Delta\eta\frac{\partial}{\partial\eta}\right](\rho q)^-$$

where q is the total velocity, $Q = \sqrt{U^2 + V^2}$ is the "modulus" of the contravariant velocity and

$$(\rho q)^- = \begin{cases} \rho q - \rho^* q^* & if \quad q > q^* \\ 0 & \quad\quad q \leq q^* \end{cases}$$

The quantities ρ^* and q^* are the sonic values of the density and total velocity.

A set of boundary conditions are imposed: zero-penetration at the body, unsteady transport equation on the wake, non-reflective conditions (in the form of Riemann invariants) at the far field.

The solution of the equation is obtained by means of the well-known Newton procedure [16]. The full potential equation is discretized as

$$L_m\left(\phi^{n+1} - \phi^\circ\right) = \frac{\left(\frac{\rho}{J}\right)^\circ - \left(\frac{\rho}{J}\right)^n}{\Delta\tau} + \left(\frac{\tilde{\rho}}{J}U\right)_\xi + \left(\frac{\tilde{\rho}}{J}V\right)_\eta - f$$

where L_m is the Jacobian system matrix, ϕ° is an intermediate guess value between ϕ^{n+1} (to be computed) and ϕ^n (already known) and f is the free stream correction term (after the discretization, eq. 2 is not satisfied if no disturbances occur in the flow). The discretization method is based on the finite-volume method described for steady flow in [17]. The numerical scheme minimizes the number of density evaluation but introduces the odd-even decoupling problem. To prevent it, a lumping operator is added to the right-hand-side.

The discretized equation is solved using an approximate factorization technique

$$L_m\left(\phi^{n+1} - \phi^\circ\right) \simeq L_\xi L_\eta\left(\phi^{n+1} - \phi^\circ\right)$$

Upwinding is applied in the L_ξ operator for improving stability which renders the bandwidth to 5 on a CH type grid.

Non-conservative formulation

The finite-difference code UFLO5, developed in [18], solves the full potential equation in non-conservative form which can be written as

$$\begin{aligned} \phi_{tt} &+ 2u\phi_{xt} + 2v\phi_{yt} = \left(a^2 - u^2\right)\phi_{xx} \\ &+ 2uv\phi_{xy} + \left(a^2 - v^2\right)\phi_{yy} \end{aligned} \tag{3}$$

where a is the speed of sound

$$a^2 = 1 - \frac{\gamma - 1}{2}\left(2\phi_t + \phi_x^2 + \phi_y^2\right)$$

Jameson's rotated scheme is applied to eq. 3 in order to account for the right domain of dependency for supersonic regions.

The boundary conditions imposed are: impermeability on the airfoil surface, zero pressure jump on the wake and a radiation condition at the far field.

In order to facilitate the application of the surface boundary conditions, the moving sheared parabolic transformation is applied to transform the physical (inertial) space coordinate system into a rectangular, equispaced body-attached coordinate system.

Compressible Unsteady Boundary Layer

All boundary layer integral methods have in common the momentum equation which is reported here with unsteady terms included :

$$\frac{1.}{\rho_e {U_e}^2}[\frac{\partial}{\partial t}(\rho_e U_e \delta^*) - U_e \frac{\partial}{\partial t}(\rho_e \theta_\rho)] + \frac{1.}{\rho_e {U_e}^2}\frac{\partial}{\partial s}(\rho_e {U_e}^2 \theta) + \frac{\delta^*}{U_e}\frac{\partial U_e}{\partial s} - \frac{C_f}{2} = 0 \quad (4)$$

where s is the distance along the wall streamline, C_f the skin friction coefficient, U is the velocity and the subscript e denotes conditions at the edge of boundary layer.
The displacement, momentum, and density thickness are defined as :

$$\delta^* = \int_0^\infty (1 - \frac{\rho U}{\rho_e U_e})dy$$
$$\theta = \int_0^\infty \frac{\rho U}{\rho_e U_e}(1 - \frac{U}{U_e})dy$$
$$\theta_\rho = \int_0^\infty (1 - \frac{\rho}{\rho_e})dy$$

In the above momentum equation, the first term is a source term and it derives from both continuity and momentum equations written in local planar coordinate system. The second term describes the rate of change of momentum thickness. The third term is the pressure gradient term while the fourth term represents the contribution coming from the shear stress.
To close the problem different equations can be chosen.
Entrainment and lag-entrainment equations have been used by some authors like Green [19] , East [20] , Cousteix [21] , LeBalleur [8] and mean-flow kinetic energy compressible equation have been used by Whitfield [9], Thomas [5], Drela [6].

The entrainment methods base equation is :

$$\frac{1.}{2\rho_e U_e}\frac{\partial}{\partial t}[\rho(H_1+\overline{H})\theta] + \frac{1.}{\rho_e U_e}\frac{\partial}{\partial s}(\rho U_e H_1 + \theta) - C_E = 0 \quad (5)$$

where C_E is the entrainment coefficient and H_1 is a shape factor equal to $H_1 = \frac{\delta - \delta^*}{\theta}$.

The energy methods base equation is :

$$\frac{1.}{2\rho_e {U_e}^2}\frac{\partial}{\partial t}[\rho_e {U_e}^2(\theta + \delta^* - \theta_\rho)] + \frac{\theta_\rho - \delta^* + \delta^{**}}{{U_e}^2}\frac{\partial U_e}{\partial t} + \frac{1.}{\rho_e {U_e}^3}\frac{\partial}{\partial s}(\rho_e {U_e}^3 \theta^*) + \frac{\delta^{**}}{U_e}\frac{\partial U_e}{\partial s} - D = 0 \quad (6)$$

with the compressibility thickness, energy thickness and dissipation integral defined as

$$\delta^{**} = \int_0^\infty \frac{U}{U_e}(1 - \frac{\rho}{\rho_e})dy$$
$$\theta^* = \int_0^\infty \frac{\rho U}{\rho_e U_e}(1 - \frac{U^2}{{U_e}^2})dy$$
$$D = \frac{1}{\rho_e {U_e}^2}\int_0^\infty \tau \frac{\partial}{\partial y}(\frac{U}{U_e})dy$$

where τ is the total shear stress.
Different authors have developed different correlations to close the problem. Here we have mainly used those derived by Green [19], and modified by East et al. [20] with reference to entrainment based methods , and those obtained by Whitfield [9], which are based on boundary layer profile family generated by Whitfield [22], with reference to energy based methods. Further details of transition, steady laminar and turbulent boundary layer solvers can be found in [2]
A 4^{th} order Runge-Kutta scheme is used to integrate the steady flow problem equations and to advance the solution in space. For unsteady flow the nature of the equations change from parabolic to hyperbolic type, the appropriate finite difference schemes used are discussed in the following subparagraph.

Unsteady formulation

We can write the resulting system of equations in compact form as :

$$\hat{A}\frac{\partial \underline{U}}{\partial t} = \hat{B}\frac{\partial \underline{U}}{\partial s} + \underline{c} = \underline{b} \quad (7)$$

where A is the $(neq \cdot neq)$ coefficients matrix (neq = number of equations present), U is the vector of unknowns and the right hand side matrix and vector contain known quantities and spatial derivatives ; manipulation of this system leads to the following final form :

$$\frac{\partial \underline{U}}{\partial t} + \hat{M}\frac{\partial \underline{U}}{\partial s} = \underline{d} \quad (8)$$

where $\hat{M} = -\hat{A}^{-1}\hat{B}$ and $\underline{d} = \hat{A}^{-1}\underline{c}$.
To solve this first order system of equations, a linear combination of the MacCormack and the Beam-Warming second order upwind scheme has been used.

This combination is necessary in order to compensate the lagging phase error typical of the MacCormack scheme and the leading phase error of the Beam-Warming scheme. Details on this analysis can be found in [23]
When the combined scheme is applied to the following system of unsteady equations,

$$\frac{\partial \underline{U}}{\partial t} = \hat{A}^{-1}\underline{b}(\frac{\partial \underline{U}}{\partial s}, \cdots) \tag{9}$$

we will obtain :

Predictor step :

$$\underline{U}_i^{\overline{n+1}} = \underline{U}_i^n + \Delta t\ \hat{A}^{-1}\ \underline{b}(\nabla_s \underline{U}_i, \cdots)$$

Corrector step :

$$\begin{aligned} \underline{U}_i^{n+1} = &\frac{1}{2}(\underline{U}_i^n + \underline{U}_i^{\overline{n+1}})+ \\ &\frac{1}{2}\Delta t\ \hat{A}^{-1}\ \underline{b}\,[\omega\, \Delta_s \underline{U}_i^{\overline{n+1}} + \\ &(1-\omega)(\nabla_s \underline{U}_i^{\overline{n+1}} + \nabla_s^2 \underline{U}_i)), \cdots,] \end{aligned}$$

where Δ and ∇ indicate forward and backward difference operators and $\omega = 1$ corresponds to MacCormack scheme while $\omega = 0$ corresponds to Beam and Warming scheme; the remainders denoted by $(\cdots)$ contains parameters such as boundary layer quantities upon which vector $\underline{b}$ is dependent.
The time step is evaluated as $\Delta t = \frac{CFL \cdot \Delta_s}{\rho(\hat{M})}$ where $\rho(\hat{M})$ is the spectral radius of matrix $\hat{M}$.
Boundary conditions are handled by introducing phantom points outside the computational domain and extrapolating the dependent variables there.
Both steady and unsteady boundary layer equations have been written and solved in direct and inverse form.

Coupling procedure

The viscous-inviscid interaction method is based on semi-inverse coupling.
The external field is solved in a direct way, while turbulent boundary layer equations are solved in inverse form starting from transition points.
Updating δ^* during viscous-inviscid interaction iterations will lead to the final converged solution. δ^* is updated during the iterations according to the relation :

$$\delta^{*(i+1)} = \delta^{*i}[1 + \omega_{coup}(\frac{U_{ev}}{U_{ei}} - 1)]$$

where ω_{coup} is a relaxation factor (about .3), U_{ev} is the velocity evaluated at the edge of the boundary layer, from boundary layer equations, and U_{ei} is the velocity from equivalent inviscid flow after that the transpiration velocity

$$V_n = \frac{1}{\rho_e}\frac{\partial}{\partial s}(\rho_e U_e \delta^*)$$

has been imposed on the wall.
On the wake no pressure variations are allowed normal to the fixed wake grid line emanating from airfoil trailing edge.
There are many possibilities to perform the coupling in unsteady computations. Up to now, only the quasi-steady interaction procedure has been implemented.
Starting from uniform flow, full potential equations are solved for a number of inviscid iterations (about 500) and zero mass flux at the wall.
In the steady case, viscous-inviscid coupling is performed and about 50 inviscid cycles per interaction are necessary to obtain an equivalent inviscid solution.
In the unsteady case, one period of oscillation is necessary to stabilize the inviscid solution and after that only at some user specified times the viscous-inviscid coupling is performed. This procedure is called ***quasi-steady coupling*** because steady-state boundary layer solution is coupled to the time-accurate solution of full potential equations.

Results and discussion

Typical C grid of 129 X 25 obtained through conformal mapping and used in the present calculations is shown in Fig. 1.

Steady case

To show the capability of the code to deal with separated flow, NLF airfoil has been analised at the pre-stall angle of attack of 14 degrees, at Reynolds number of 4 million and at a Mach number of .1.
Fig. 2 shows the comparison between viscous results obtained with FPNC code along with experiments [26]. The agreement between numerical results with experiments is quite satisfactory.

The transonic steady experimental results for a NACA0012 airfoil obtained by Mc. Devitt and Okuno, [27] have been used for comparison with numerical results.
In Fig. 3 comparison between inviscid solutions obtained with FPNC and FPC codes for $\alpha = 2.$ $M = .755$ are shown along with experiments obtained at $Re = 10\ Ml$. It can be clearly seen that inviscid FPNC computations agree quite well with experiments showing that they are inaccurate for the case

under investigation; in fact because this is a strong shock wave case, artificial numerical dissipation employed in the inviscid numerical scheme, is such that it weakens shock wave while the *real* inviscid flow is better represented by FPC results which are very similar to Euler computations. This is why the FPNC codes have been so popular in the industry in the recent past.
Viscous solutions are reported in Fig. 4 for the same airfoil with $\alpha = 2.$ $M = .750$, $Re = 14\ Ml$, showing that the coupling procedure is effective in predicting shock position even if in this strong shock case the intensity of the shock is overpredicted; we should also take in account that no corrections have been applied on experimental Cp.
As far as concern compressible and turbulent boundary layer methods, in Fig. 5 are reported solutions obtained with FPC code coupled to two different steady boundary layer methods.
In particular Green method [19], (as modified by East et al.[20]) is compared to Whitfield [9] energy method which causes a little forward movement of shock.
All boundary layer methods available in the present version of the code, are compared among them for a shock wave-boundary layer interaction as experimented by Kooi [28]. The results are shown in Fig. 6 where the displacement thickness distribution shown, and used as input for the inverse boundary layer computation, is that measured experimentally by Kooi. The oscillation in the distribution have been left on purpouse in order to see if any of the tested methods presents a kind of *smoothing effect.* As it can be inferred from the figure, equlibrium kinetic energy model as proposed by Thomas [5], presents this effect. As far as concern incipient separation prediction (as observed by Kooi in his experiment) all of them are able to predict it, meaning that when δ^* is correctly evaluated all the rest is well predicted.

Unsteady case

Unsteady boundary layer

In fig. 7 direct and inverse unsteady boundary layer solution is obtained for a case proposed by Cousteix; this is an incompressible test case in which a linear velocity gradient variable with time is imposed on a flat plate. Details can be found in [21] In particular the shown disribution of $U_e(x,t)$ is imposed for the direct boundary layer solution and $\delta^*(x,t)$ is obtained. Then imposing this $\delta^*(x,t)$ distribution for the inverse method, the same $U_e(x,t)$ as for the direct case should be obtained. As it can be seen from the figure the results are correct. For this case a wheighted factor of $\omega = .5$ has been used in the combined numerical scheme to solve the unsteady system of equations.

Furthermore the numerical results obtained (not shown in the paper) agree quite well with those shown in the Cousteix paper [21].

Agard test case 1

The standard Agard test case 1, as reported in [29], has been used for numerical comparison. Case 1 is relative to a Naca 0012 airfoil undergoing a pitching motion with the following law : $\alpha = 2.89 + 2.41\, sin\,(\omega t)$ with a freestream $Re = 4.8\ Ml$ and a reduced frequency $k = \frac{\omega c}{2V} = .0816$.
Up to date the unsteady coupled solutions obtained and shown in the paper, use as inviscid solver the FPNC code while the coupling of unsteady FPC code with boundary layer is under development.
Fig. 9 reports a comparison between C_l obtained from FPNC inviscid and viscous code. It can be seen that the effect of viscosity is to lower the Cl values during the cycle and also to understimate these values specially in the downstroke movement.
In fig. 8 and fig. 10 it is shown the comparison between numerical and experimental pressure coefficient distributions at specified angles which are the same of those reported in [29]. This attempt to compare numerical pressures to those measured is just to have an idea of what is going on, because no correction is applied neither to pressure coefficients nor to angles of attack.
As already said, during the angle of attack decreasing phase, there is an underprediction of loads.
Fig. 11 and fig. 12 shows frequency effect. In figures 11 and 12 the results obtained from the FPNC inviscid and viscous codes at nominal and double frequency are reported respectively. It can be seen that the viscous solution tends to cancel the frequency effect. The reason for this is under investigation.

Agard test case 5

Case 5 is relative to the same NACA 0012 airfoil undergoing a pitching motion with the law :
$\alpha = 0.016 + 2.41\, sin\,(\omega t)$ with a freestream $Re = 5.5\ Ml$ and a reduced frequency $k = .0816$. In Fig. 13 inviscid and viscous C_l cycles are reported as obtained from FPNC code along with experiments and it is clear that, for this strong shock case, the FPNC code results are totally inaccurate and the need of a better inviscid solver, such as Helifp, is urgent.

A typical inviscid calculation for a complete cycle of oscillation for a standard $129\,X\,25$ grid takes about 30 minutes on a Convex C38 mainframe for the FPNC code. When viscous runs are performed, the total required time increases of about 30% of the corresponding time needed for the inviscid solutions.

Conclusions

This paper has presented a study of unsteady compressible viscous and transonic flows. This has been done using viscous-inviscid interaction technique and using full potential equations in both conservative and non conservative form as inviscid solver. For the unsteady coupled solution, only non conservative full potential formulation has been used. As a boundary layer solver the unsteady and compressible integral boundary layer equations have been coded and results obtained using different methods have been compared with experimental data. The quasi-steady interaction procedure has proved to be accurate enough when the oscillation frequency is not too high and when the shock waves are not too strong. True unsteady coupling is currently under development. This work is a first step in an attempt to predict complex unsteady transonic flows.

Acknowledgement

The HELIFP code is being developed within the HELISHAPE project by ONERA, CIRA, DRA, NLR, Politecnico di Milano, Agusta, ECF, GKN Westland Helicopters and is funded by the European Union under the BRITE/EURAM program.
The authors whish to thank the graduate student Biagio Imperatore who run some of the mentioned codes obtaining many of the presented results.

References

[1] Coiro, D.P., Amato, M., and de Matteis, P., "Numerical Prediction of Transonic Viscous Flows Around Airfoils Through an Euler/Boundary Layer Interaction Method," AIAA Paper 90-1537, June 1990.

[2] Coiro, D.P., de Matteis, P., and Amato, M., "Wake Effects on the Prediction of Transonic Flows Around Airfoils With an Euler/Boundary Layer Interaction Approach", Journal of Aircraft, Vol. 29, Num. 3, May-June 1992

[3] Lock, R.C., Firmin, M.P.C., "Survey of techniques for estimating viscous effects in external aerodynamics," *Numerical Methods in Aeronautical Fluid Dynamics*, Ed. P.L. Roe, Academic Press, 1982, pp. 337-430.

[4] Melnik, R.E., Chow, R.R., Mead, H.R., and Jameson, A., "An Improved Viscid/Inviscid Interaction Procedure For Transonic Flow Over Airfoils," NASA CR-3805, October 1985.

[5] Thomas, J.L., "Transonic Viscous-Inviscid Interaction using Euler and Inverse Boundary Layer Equations," Ph.D. Thesis, Mississipi State University, 1983.

[6] Drela, M., "Newton Solution of Coupled Viscous/Inviscid Multielement Airfoil Flows," AIAA Paper 90-1470, June 1990.

[7] Fenno, C.C., Newman, P.A., and Hassan, H.A., "Unsteady Viscous-Inviscid Interaction Procedures for Transonic Airfoils Using Cartesian Grids, " paper 88-2591-CP, AIAA 6^{th} Applied Aerodynamic Conference, Williamsburg, VA, 1988

[8] Le Balleur, J.C., and Girodroux-Lavigne, P., "A viscous-Inviscid Interaction Method for Computing Unsteady Transonic Separation, " Third Symposium on Numerical and Physical Aspects of Aerodynamic Flows, California State University, 1985, (ONERA T.P. No. 1985-5)

[9] Whitfield, D.L., Swafford, T.W., and Jacocks, J.L., "Calculation of Turbulent Boundary Layers with Separation and Viscous-Inviscid Interaction," *AIAA J.*, Vol. 19, No. 10, October 1981.

[10] Henke, H., and Muller, U.R., "Progress in Unsteady Transonic Viscous-Inviscid Computational Methods ", International Forum on Aeroelasticity and Structural Dynamics, Strasbourg, France, 1993

[11] Houwink, R., "Computation of Unsteady Turbulent Boundary Layer Effects on Unsteady Flow About Airfoils, " Fourth Symposium on Numerical and Physical Aspects of Aerodynamic Flows, Jan. 1989

[12] Dini, P., Coiro, D.P., and Bartolucci, S., " Vortex Model for Airfoil Stall Prediction Using an Interactive Boundary-Layer Method " ASME Congress, USA, February 1995

[13] Howlett, J.T., "Efficient Self-Consistent Viscous-Inviscid Solutions for Unsteady Transonic Flow, " J. of Aircraft, Vol. 24, Num. 3, November 1987

[14] Hounjet, M., "Full Potential Models Proposed by NLR for a Single Blade Rotorcraft code; contribution to BRITE/EURAM Project 'HELISHAPE': Task 2.2 (Formulation)," NLR CR 94380 L, 1995.

[15] Costes, M., Hounjet, M.H.L., Kokkalis, A., Gasparini, L., Vigevano, Pagano, A., Spruce, M., Miller, J.V., "Activities Completed During The First Eighteen Months of HELISHAPE Task 2," ONERA Technical Report RT 190/1369 AY, April 1995.

[16] Ide, H. and Shankar, V.J., "Unsteady Full Potential Aeroelastic Computations for Flexible Configurations," AIAA paper 87-1238, 1987.

[17] Jameson, A. and Caughey, D.A., "A Finite Volume Method for Transonic Potential Flow Calculations," AIAA paper 77-635, 1977.

[18] Chang, I.C., "Unsteady Transonic Flow Past Airfoil in Rigid Body Motion," Ph. D. Dissertation, Courant Institute of Mathematical Sciences, New York University, 1980.

[19] Green, J.E., Weeks, D.J., and Broman, J.W.F., "Prediction of Turbulent Boundary Layers and Wakes in Compressible Flow by a Lag-Entrainment Method," R.A.E. TR 72231, 1972.

[20] East, L.F., Smith, P.D., and Merryman, P.J., "Prediction of the Development of Separated Turbulent Boundary Layers by the Lag-Entrainment Method, " R.A.E. TR 77046, 1977

[21] Cousteix , J., Houdeville, R., et Dessoper, A., "Resultats Experimentaux et Methodes de Calcul Relatifs aux Couches Limites Turbulentes en Ecoulment Instationnaire, " AGARD Conference on Unsteady Aerodynamics, CP-227, Ottawa, 1977

[22] Whitfield, D.l. "Analytical Description of the Turbulent Boundary Layer Velocity Profile" AIAA paper 77-1158, 1978.

[23] Pirzadeh, S., and Whitfield, R., "Three-Dimensional Unsteady Transonic Viscous-Inviscid Interaction Using the Euler and Boundary-Layer Equations, " paper 88-2578-CP, AIAA 6^{th} Applied Aerodynamic Conference, Williamsburg, VA, 1988

[24] Carter, J.E., "A New Boundary Layer Inviscid Interaction Technique for Separated Flows," AIAA Paper 79-1450.

[25] Lighthill, M.J., "On displacement thickness," *J. of Fluid Mechanics*, Vol. 4, Part 4, 1958, pp. 661-663.

[26] Somers, D.M., "Design and Experimental Results for a Natural-Laminar-Flow Airfoil for General Aviation Applications " NASA TP-1861, 1981

[27] Mc Devitt, J.B., and Okuno, A.F., "Static and Dynamic Pressure Measurements on NACA 0012 Airfoil in the Ames High Reynolds Number Facility, " NASA TP-2485, June 1985

[28] Kooi, J.W., "Experiments on Transonic Shock-Wave Boundary Layer Interaction, " Agard CP-168, paper 30, 1976

[29] Landon, R., "NACA 0012 Oscillatory and Transient Pitching, " Compendium on Unsteady Aerodynamic Measurement, AGARD-R-702, 1982

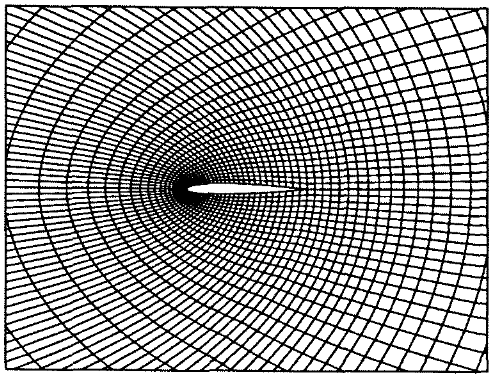

Figure 1: C grid around NACA0012 airfoil
129 X 25 grid points

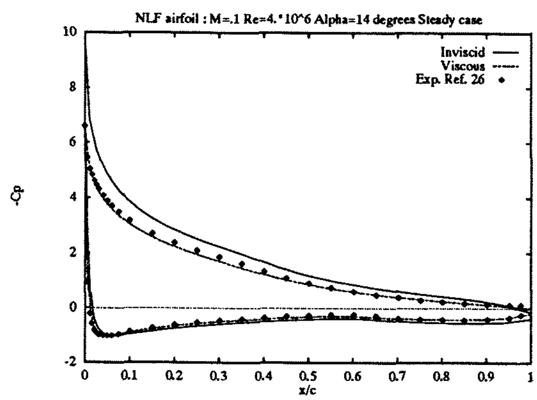

Figure 2: Chordwise pressure distribution on NLF at Mach = 0.1, $\alpha = 14.0°$, Re = 4.E06

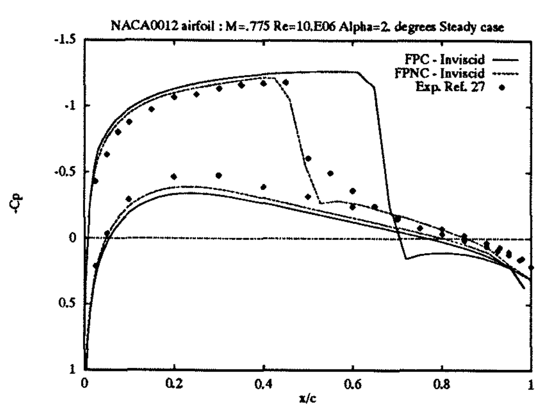

Figure 3: Chordwise pressure distribution
NACA0012 Mach=0.775, $\alpha = 2.0°$, Re=10E06

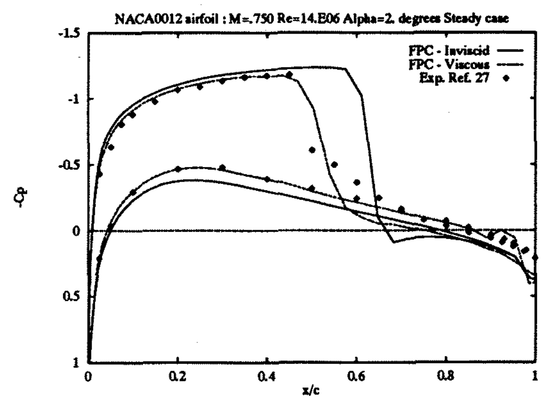

Figure 4: Chordwise pressure distribution
NACA0012 Mach=0.750, $\alpha = 2.0°$, Re=14E06

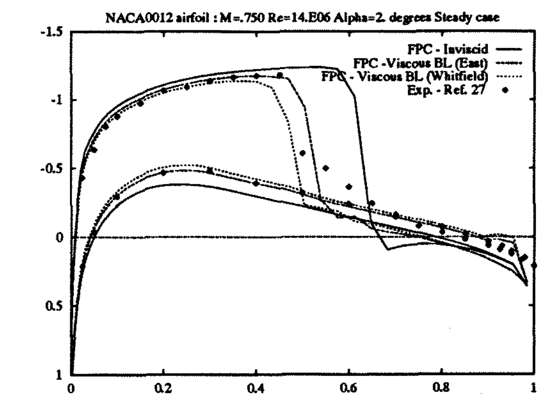

Figure 5: Effect of b.l. methods on pressure distribution
NACA0012 Mach=0.750 $\alpha = 2.0°$, Re=14E06

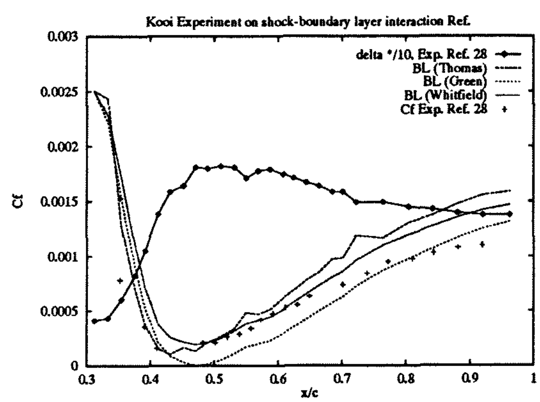

Figure 6: Effect of b.l. method on shock-boundary layer interaction, Kooi case, [28]

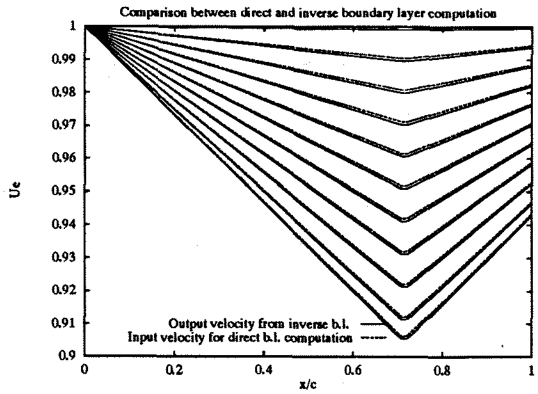

Figure 7: Comparison of direct and inverse boundary layer solutions
Unsteady velocity distributions, [21]

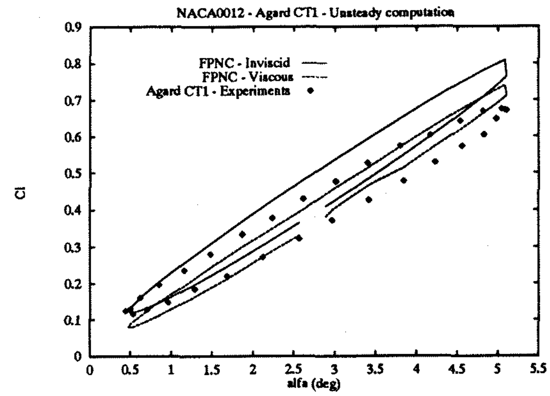

Figure 9: Lift coefficient variation with regard to unsteady pitching angle
NACA0012-Agard CT1-Ma=0.600,Re=4.8E06
$\alpha^\circ = 2.89 + 2.41\, sin(.081\, t)$

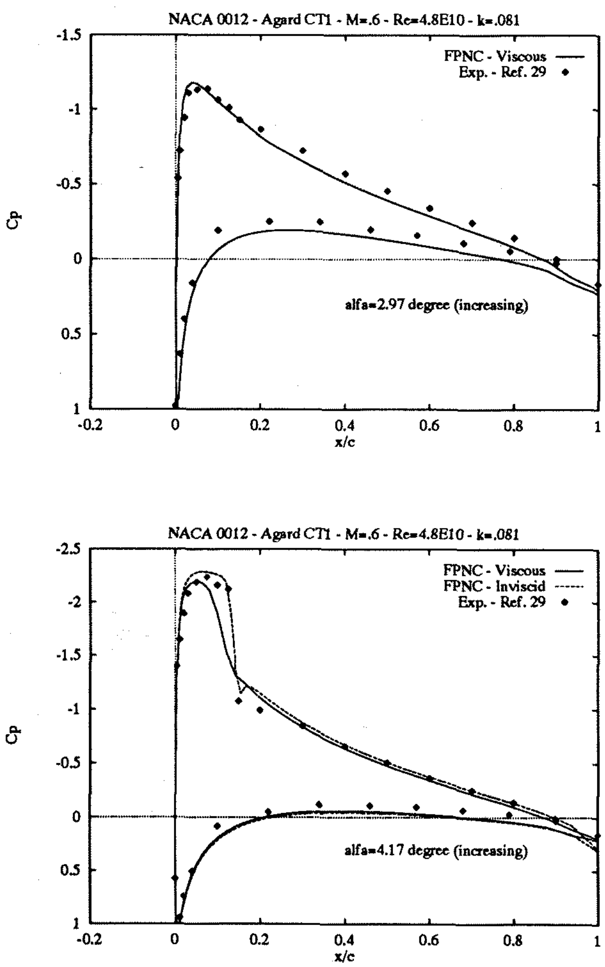

Figure 8: Unsteady Surface Pressure Coefficient
NACA0012-Agard CT1-Ma=0.600,Re=4.8E06
$\alpha^\circ = 2.89 + 2.41\, sin(.081\, t)$, increasing angles

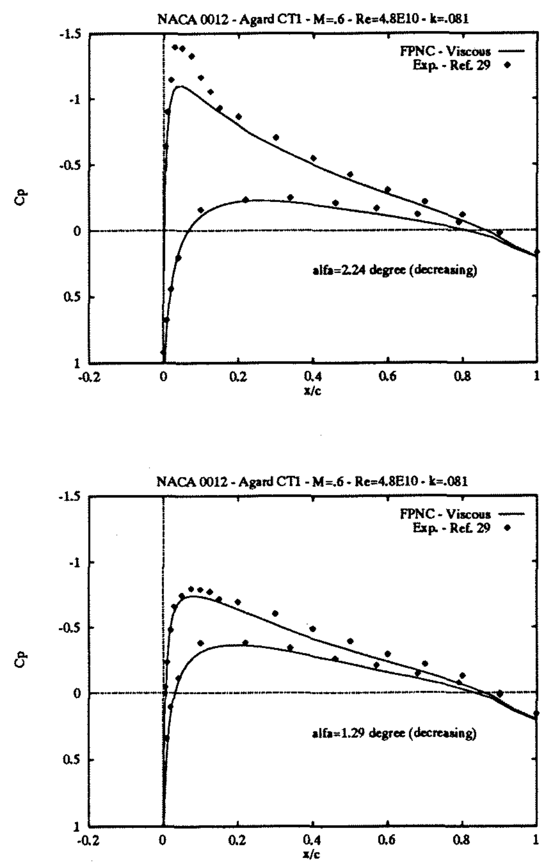

Figure 10: Unsteady Surface Pressure Coefficient
NACA0012-Agard CT1-Ma=0.600,Re=4.8E06
$\alpha^\circ = 2.89 + 2.41\, sin(.081\, t)$, decreasing angles

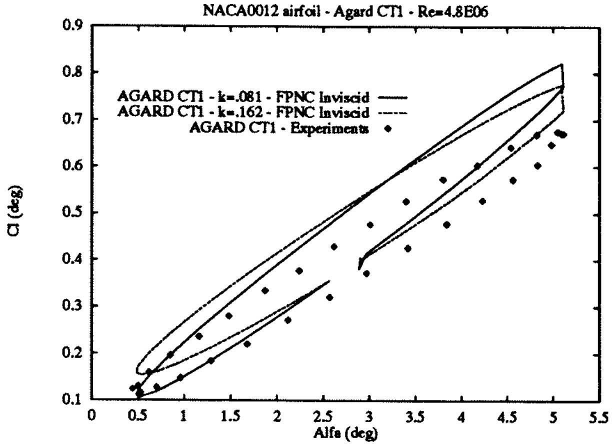

Figure 11: Variation of numerical inviscid lift coefficient for two values of the reduced frequency

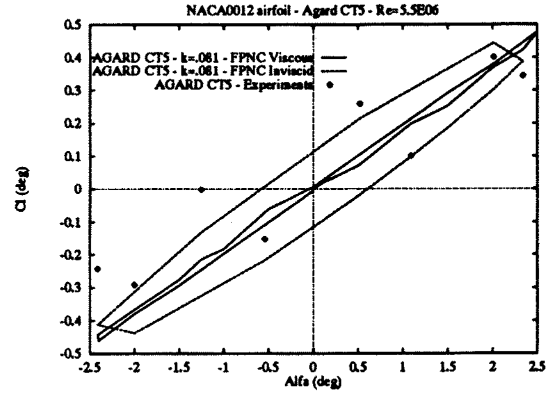

Figure 13: Lift coefficient variation with regard to unsteady pitching angle
NACA0012-Agard CT5-Ma=0.755, Re=5.5E06
$\alpha^{\circ} = 0.016 + 2.51\, sin(.081\, t)$

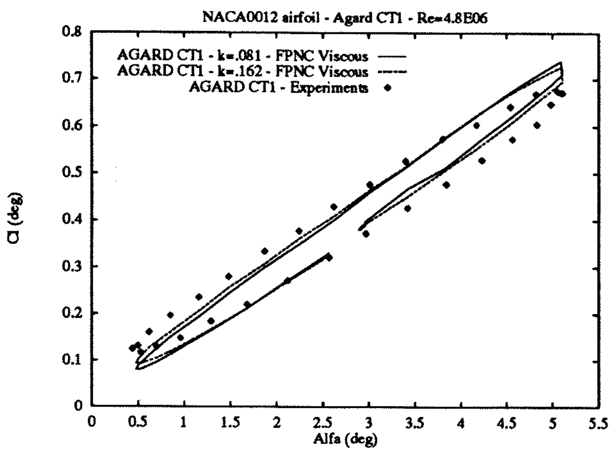

Figure 12: Variation of numerical viscous lift coefficient for two values of the reduced frequency